DOI: 10.13009/EUCASS2022-6087

Numerical Simulation of the Roughness Effects on the Asymmetric Flow over Axisymmetric Bodies

José Jiménez-Varona, Gabriel Liaño and José L. Castillo, Pedro L. García-Ybarra***
**PhD Research Scientists, Flight Physics Department, INTA*
Carretera de Ajalvir km 4,5 28850 Torrejón de Ardoz, Madrid, Spain, jimenezj@inta.es, liagno@inta.es
***Professors, Faculty of Sciences, Universidad Nacional de Educación a Distancia, UNED*
Avda. de Esparta s/n, 28232 Las Rozas, Madrid, Spain, jcastillo@ccia.uned.es, pgybarra@ccia.uned.es

Abstract
The flow at high angles of attack over axisymmetric configurations is not symmetric. The mechanism that triggers this asymmetry may be the combination of a global instability and a convective instability due to irregularities of the configuration.
Additionally, the flow structure is very complex: it involves large separated flow regions, and a complex vortex sheet structure. The numerical prediction is then very difficult, even using high fidelity flow solvers and advanced turbulence models for this simple configuration. For this case, the roughness and other geometrical minute imperfections are of paramount importance in the resultant flow field and the forces past the body. Therefore, this roughness has to be taken into account in the numerical calculations.
For the numerical prediction of the flow about a missile type configuration, how the body surface is modelled is therefore very relevant; especially the tip zone of the body. For this reason, two grids were built up. One structured grid -inherently axisymmetric- and one unstructured grid, not symmetric, with irregularities that resemble a rough model. Previous studies conducted at a high angle of attack with Reynolds Stress Turbulence models (RSM) showed asymmetric flow with no orientation angle effects for the structured grid, while there were important differences in the global forces if the unstructured grid was used. This grid has some kind of numerical roughness which resembles a rough model. But, there were difficulties in the simulation: the observed damping of the forces in the rear part of the body was not calculated accurately with the RSM model. And the unsteady flow detected in this part - experimentally and also with Detached Eddy Simulation codes (DES) - was also not predicted.
An alternative calculation using an advanced turbulence model has been carried out. The Scale Adaptive Simulation (SAS) model developed by Menter and Egorov has demonstrated to be superior to other typical eddy-viscosity or Reynolds Stress turbulence models. A validation of the method has been conducted at a high angle of attack using abundant experimental information of an ogive-cylinder configuration at subsonic flow conditions. The theoretical results are in consonance with the experimental data. This validation was extended to studies of the influence of roughness in the global coefficients and of the angle of attack for onset of asymmetry for either a smooth or a rough body, resembled respectively with the structured and the unstructured grids. The theoretical solutions show fair agreement with the experimental data, indicating a good capability of URANS methods -provided RSM-SAS turbulence model is used- in achieving an accurate prediction of the flow field at high angle of attack and subsonic flow conditions.

1. Introduction

The numerical simulation of the flow field past an axisymmetric body flying at high angle of attack and subsonic flow conditions is a challenging problem, since it entails large areas of boundary layer separation and a complex vortex sheet structure. At low angles of attack the dominant axial flow component keeps the flow attached to the body, developing a normal force which increases linearly with the angle of attack. At intermediate angles the increasing adverse pressure gradients on the body surface force the leeside boundary layer to separate, yielding a steady symmetric vortex pair. The normal force then evolves in a nonlinear manner, but there is still no side force. At larger angles of attack the vortices become asymmetric leading to the appearance of a side force and a complex unsteady flow pattern at the rear. At very large angles the axial flow component has little influence and the boundary layer is shed in an

DOI: 10.13009/EUCASS2022-6087

unsteady fashion, similar to the wake behind a two dimensional cylinder normal to the flow, the average side force decaying to zero.
There are two dimensionless parameters of the flow domain that affect this basic flow structure: Mach number and Reynolds number. Regarding the Mach number, the asymmetry of the flow disappears as the Mach number increases. The appearance of shocks at the leeward side makes the flow symmetric [1]. Concerning Reynolds number effects, it has been demonstrated in several experimental tests that maximum side forces occur both at laminar or turbulent flow conditions. This behavior reinforces the idea that a global instability of inviscid nature is the origin of the asymmetry [1]. Experiments conducted by Lamont [2] showed this effect: the side forces are reduced in the critical Reynolds number region.
Moreover, some geometric characteristics are relevant for the flow structure: nose angle, bluntness, fineness ratio and roughness. The nose angle appears to be a relevant factor. Keener and Chapman [3] introduced the idea of a hydrodynamic (inviscid) mechanism as the origin of the asymmetry. The asymmetric wake is the result of an inviscid instability that occurs when two vortices are "crowded together" near the tip of the body. One vortex moves away from the body and the other moves underneath the first. Champigny [1] showed that above a certain angle of attack, very small perturbations (inhomogeneity in the mainstream, surface irregularities, geometrical defects, etc.) are sufficient to cause the vortex system to go from an unstable symmetric state to a stable asymmetric structure. Different experimental tests for ogives or cones have shown an empirical correlation between the angle of attack for onset of asymmetry and the semi apex angle δ_n, such that: $\alpha_{onset} = 2 \cdot \delta_n$ [4]. This value is reduced as the fineness ratio increases [1], indicating an instability due to the afterbody.
Roughness or small eccentricities or other geometrical body imperfections are also relevant factors in the appearance of asymmetric flow patterns. At a certain angle of attack, experiments have shown that the side forces depend on the orientation angle [1], [4], [5], [6], [7], [8]. Two different series of experiments, one described by P. Champigny on an ogive cylinder configuration (references [1], [6]) and other conducted by Mahadevan *et al.* on a cone configuration (reference [7]),reported orientation angle dependent side forces, due to the roughness of the model. The results for the ogive cylinder showed a bi-stable behavior for smooth surfaces while for a rough surface the side force depended on the orientation angle, leading to large variations of the side force magnitude. Similarly, the results of the rough surface model of a cone [7] showed a sinusoidal variation of the side force with the orientation angle, while there was a bi-stable pattern of the side force –either negative or positive of similar magnitude- at the range of moderate to high angles of attack for the smooth surface model.
Experiments conducted by Kruse, Keener and Chapman [5] showed that rotating the tip of an axisymmetric body has large effects on the side forces; the rotation of the afterbody (cylindrical part) holding the tip had also a large effect on these side forces. Then, minor surface irregularities may cause the activation of a convective instability, also in zones far from the tip. The result is a dependence of the side force on the orientation angle.

From a numerical point of view, the study of the flow field past axisymmetric bodies at high angle of attack has been demonstrated to be very difficult, since it entails large areas of boundary layer separation and a complex vortex sheet structure. Additionally, two or three different flow regions have been detected, with a fluctuating flow in the rear part, leading to a von Karman vortex street type flow region in the rear part of bodies of high fineness ratio [9]. The increment of the fineness ratio –increasing the cylindrical body for example while holding the nose- leads to an increment of the instability of the flow at similar angles of attack.
Thus, the numerical simulation is a challenging problem: it involves unsteady flow, large separated flow regions, and a complex vortex sheet structure. This problem of numerical simulation has been afforded since the last decade of the past century. As the URANS methods became more developed, and the computational capability was increased, the accuracy of the numerical solutions increased. An important assessment of numerical methods using different Computational Fluid Dynamics (CFD) codes and different grids, either structured or unstructured grids, is shown in the reference [10]. This is the final report of a GARTEUR Action Group (AG (AD) 42) related to missile type configurations. The theoretical solutions of different CFD codes, that also used different turbulence models, were compared to the experimental information available for an ogive-cylinder configuration tested at subsonic flow conditions at several wind tunnels in 1982 [11].
The conclusions of the theoretical computations showed poor agreement of the one-equation eddy viscosity turbulence models, as the well-known Spalart-Allmaras model, which led to symmetric flow at a high angle of attack as large as 45 degrees, where the flow is asymmetric and the experimental data showed an important side force value with a sinusoidal form of the local side force. Two-equation eddy viscosity models, as the *k-ω* turbulence model, seemed to provided better accuracy, but only Detached Eddy Simulations (DES) or Large Eddy Simulations (LES) solutions could capture a damping of the local forces at the rear in consonance with the experimental information. Additionally, these codes obtained unsteady solutions with a dominant frequency, when making a Power Spectral Density (PSD) analysis of the forces. There was a concern regarding the mesh density, the turbulence models and also with the algorithms employed for the convective fluxes. A calculation using Spalart-Allmaras turbulence model achieved a

DOI: 10.13009/EUCASS2022-6087

symmetric flow solution when using a numerical scheme Roe of first order, while the solution was asymmetric if a third order scheme was used [10].
Therefore, taking into account these difficulties it was necessary to continue the assessment of CFD codes, and also to check the grids used for the calculations. The grids must be of large size, with a large grid density. The problem of roughness detected in the experimental tests should be taken into account when making the calculations, and some way for measuring the relative roughness is needed when comparing the theoretical calculations with the experimental tests. Many experiments have been conducted for a polished or rough model of the same configuration [1], [4], [7], [11], showing different solutions at high angles of attack, as a result of the convective instability.
When starting studies for this type of configurations at subsonic flow conditions and high angles of attack, the authors chose the ogive-cylinder configuration studied in the GARTEUR Group AG (AD) 42 (see [10]) as the reference configuration, due to the abundant information at angle of attack of 45 degrees –global forces, local forces and pressure at several sections- and information of the global forces at a wide range of angle of attack for two models: polished and rough models ([1], [10], [11]). The preliminary results of these calculations and their comparison with experimental data are given in reference [12], a paper presented at 8th EUCASS Congress celebrated in July 2019 in Madrid (Spain). An important conclusion obtained after these calculations, was that Reynolds Stress turbulence models (RSM) obtained better solutions than eddy-viscosity turbulence models, leading to an increment of both the side and normal forces, and these values approximated better to the experimental values. But, even using the high level turbulence models (RSM), the local force solutions at the rear showed poor agreement with the experiments –showing little damping of the local forces- and the calculations led to steady solutions, not capturing the unsteady flow region at the rear. In reference [10] only LES or DES codes could obtained these features of the flow.
Some authors have remarked that most of the Unsteady Reynolds Averaged Navier-Stokes (URANS) methods have proven not to be capable to correctly predict the flow field. The reason is that they do not display the correct spectrum of turbulent scales, even if the numerical grid and the time step would be of sufficient resolution [13]. URANS methods are overly dissipative and resolve only frequencies far lower than those of turbulent fluctuations [14].
On the other hand, for wall boundary layers, the turbulence length scale becomes very small relative to the boundary layer thickness. For high Reynolds numbers, this poses severe limitations for LES models. The computational effort compared to URANS methods may increase in several orders of magnitude [13]. Calculations with LES codes using very fine meshes and reduced time steps limited absolutely their use taking into account the computational capabilities of our Institution.

Therefore, the study was conducted in another way that has been fruitful. The use of Scale Adaptive Simulation (*SAS*) implemented in ω-based turbulence models by Menter *et al.* [13], [14], [15], [16], [17].
A summary of the features of SAS is given in [14]: "SAS is an advanced URANS model which can produce spectral content for unstable flows". The method is based on the introduction of a second length scale into the turbulence model, either a *k-ω SST* turbulence model, or a ω-based Reynolds Stress turbulence model (*ω-RSM*) [17]. This length scale is the von Karman length scale L_{vk} . This length scale adjusts to the smallest scales and produces an eddy viscosity small enough to allow the formation of even smaller eddies until the grid limit is reached [14]. Thus, *SAS* has a LES-like behavior in unstable regions of the flow and it works in RANS mode in the stable zones. It is worth noting that Menter and Egorov mention that "the ability of SAS to adjust the eddy-viscosity to the resolved scales is unique and cannot be achieved with standard LES models" [15]. If the grid is coarse or large time steps are used *SAS* model will run in RANS mode. One drawback of SAS model is that it relies on an instability of the flow to generate resolved turbulence. In case such an instability is not present, the model will remain in RANS mode [15]. This is the main concern relative to *SAS*. It is reported in reference [14] that the unsteady behavior of the flow past a backward facing step was not achieved with *SAS*. *SAS* will not switch into scale-resolving mode if the flow is not sufficiently unstable [14].
The assessment and validation of the theoretical calculations with regard to the experimental data consisted of conducting a study using *SAS* method, implemented in the *ANSYS FLUENT*© code [17]. The results were qualitatively and quantitatively better than those solutions obtained by eddy-viscosity models or by standard Reynolds stress models (RSM). An important issue of this study is that *k-ω SST SAS* model was not sufficient for capturing the unsteady flow region in the rear, which led to a damping of the averaged local forces. The model that achieved accurate solutions was only the *RSM-SAS* model. A description of the comparison between three different turbulence models and the experiments is given in a paper of the authors [24].
The calculations were done using two different grids, one structured axisymmetric grid, and another unstructured grid, which was intrinsically non symmetric. The departure of the symmetric feature for the surface mesh is very important, due to the fact that roughness effect is of paramount importance in the flow field. Several tests showed differences in the side force up to 50% in magnitude, depending on whether the model is polished or not [1], [4], [7].

In this paper, we will focus on the large differences in the flow field due to the roughness effect, demonstrated in the experiments, and also obtained with theoretical solutions, either using a structured axisymmetric grid -which resembles a polished model-, or an unstructured grid, with sufficient numerical roughness to resemble a rough model. A

DOI: 10.13009/EUCASS2022-6087

measurement of the numerical roughness was done and compared with the available information of roughness for the test model.
The effect of the asymmetry –small imperfections- of the unstructured grid is to produce a convective instability which adds to a global instability at high angles of attack. The main conclusion of the comparison of both theoretical solutions is an orientation angle dependence of the forces for the unstructured grid, and also a premature angle of attack for onset of asymmetry regarding the angle of attack for onset of asymmetry achieved with the structured grid.
There is no experimental information on the orientation angle dependence for the forces, but the experimental data of the forces at different angles of attack showed that the angle of attack for onset of asymmetry for the rough model was much lower than that of the polished model. Bot structured and unstructured grids solutions were in consonance with the experiments, indicating a good capability of prediction.
In the following chapters, a brief description of the validation and assessment of the turbulence model is shown, together with a comparison of the theoretical solutions with the experimental solutions.

2. Configuration and test conditions: Ogive-cylinder

A configuration with abundant experimental data was used as test case. Thus, our numerical results are compared to the experimental data of an ogive-cylinder configuration tested by ONERA (Office National d'Etudes et de Recherches Aérospatiales) [10], [11]. The test model consisted of a 120 mm diameter cylindrical body with a 3-calibre tangent ogive nose. The total length was 15 calibers (*L/D=15*). This ogive-cylinder configuration was tested in the ONERA F1 pressurized wind tunnel at Le Fauge-Mauzac (France). The flow conditions for the reference case were Mach number Ma = 0.2, Reynolds number Re = $2 \cdot 10^6$ and angle of attack $\alpha = 45.43$ degrees. Results at other angles of attack were also available.
The diameter of the configuration under study was D = 1 m. The temperature of the air was T= 288 ºK and the pressure and density were adjusted to obtain a Reynolds number similar to that of the experiments. For the theoretical study, the reference case flow conditions were Mach number Ma = 0.20, Reynolds number Re = $2.2 \cdot 10^6$ and angle of attack $\alpha = 45.00$ degrees. Also, a sweep in angle of attack was done, from low values and up to 45 degrees.
A theoretical study using different codes with several turbulence models and different grids was done under a *GARTEUR* Research Group, led by Prananta [10]. This study has been very useful for the present work and helped to do the comparison with the experimental data and to obtain conclusions about the different turbulence models. A sketch of the model, with the location of pressure taps is given in Figure 1 (reprinted from reference [10]).

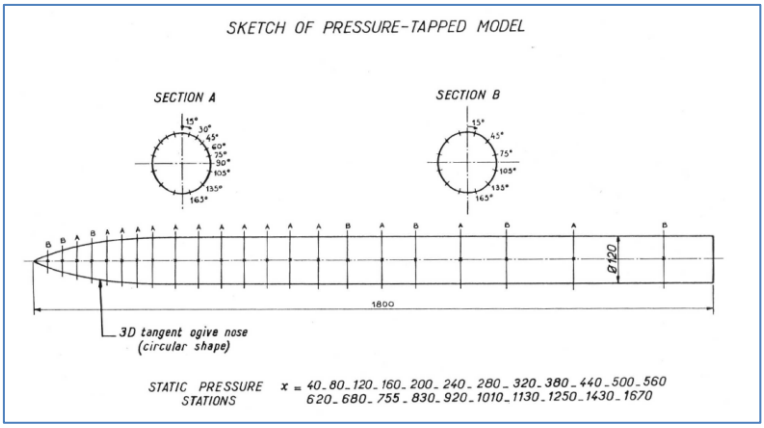

Figure 1: Sketch of the GARTEUR AG04 missile geometry and pressure taps (reprinted from [10]).

3. Grids: Numerical Roughness

All the experimental information available relies on the paramount importance of the roughness and surface imperfections in the production of a convective instability which leads to an orientation angle dependence of the forces with a large variation in magnitude of the side force mainly. This is added to a global instability which happens at a certain angle of attack where the flow changes from an unstable symmetric flow solution to a stable asymmetric flow solution. Then, a question to be answered was: is it possible to compute the roughness and imperfections effects such that important differences in the theoretical solutions can be obtained in a similar fashion as it is found in the wind tunnel tests?
Two grids were generated for such purpose.

DOI: 10.13009/EUCASS2022-6087

The first one is a structured axisymmetric grid and the other is an unstructured hybrid grid, composed by prismatic and tetrahedral elements.
Regarding the structured grid, a two-dimensional structured grid was built up. Then, this planar two-dimensional grid was rotated about the longitudinal axis every *n* degrees. The total number of cells in azimuth direction is $360/N$. This number *N* was chosen as 240 or 360. The grid with 240 cells in azimuth direction was the grid utilized as reference grid for the calculations. The structured grid finally used has 450 cells in the longitudinal direction (x-axis direction), 140 in normal direction and 240 in azimuth direction. This grid resembles a smooth axisymmetric body with a very small irregularity in the tip which is symmetrically distributed. It is a fine mesh of 15120000 cells and 45114720 faces. There are small irregularities of the curvature in the tip but uniformly distributed. A detail of the surface grid at the nose and the grid in a transverse plane is given in Figure 2.

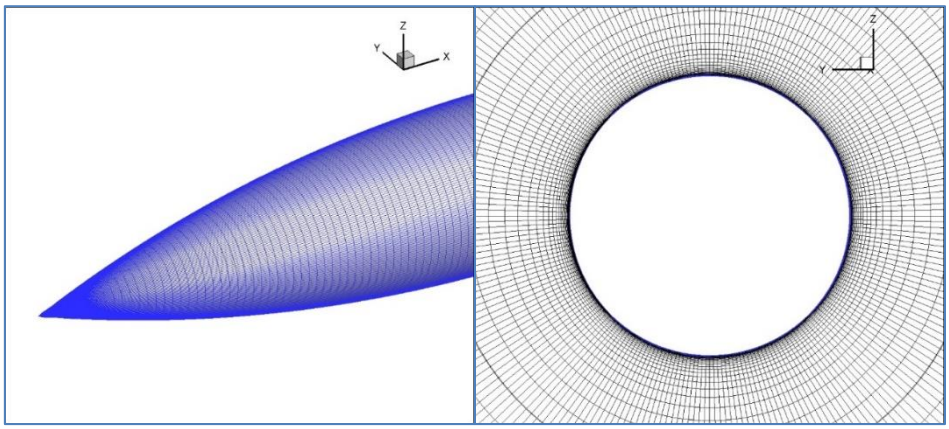

Figure 2: Detail of the structured grid: Left: Surface mesh on the nose. Right: Transversal plane y-z.

The unstructured grid was built up with a very different methodology, using a method to generate a surface mesh of a part of the ogive-cylinder covered by an angle $\Theta = 360/m$ -being *m* an integer. This integer *m* can have different values. Values ranging from *m = 3* to *m = 8* have been used for the calculations. A maximum cell size is chosen, together with other parameters. This method implies that in the sections x/D very close to the tip, the grid is formed by a triangle if *m = 3* and by an octagon if *m = 8*. When advancing in longitudinal direction a cross section will be formed by polygons of many elements which are closer to the ideal circular shape of the body in these sections. With the structured mesh, every section was formed by 240 or 360 elements, independent of the radius of the circular section. For this unstructured mesh, these polygons have different number of elements and their distribution is not regular. The result is a surface mesh not axisymmetric, with cross sections different in number and distribution of the elements.

To give an insight of the implications of this type of meshing, a detail of the tip region is shown in Figure 3 for values of *m = 3* and *m = 8*. The tip of the coarse mesh built up with *m = 3* is very irregular. The tip of a grid generated with *m = 8* is more regular but not axisymmetric. Finally, the finer grid of the right looks more symmetric; but, a detailed insight shows differences at each orientation angle. Therefore, neither of these grids are symmetric in the same fashion than the previously described structured grid. The finer grid was chosen for the computations. It has 16240213 cells, with 48 prismatic layers.

It is interesting to show the surface grid in sections close to the tip. It can be seen in Figure 4 (left plot) -in the sections from x/D = 0.001 to x/D = 0.005- that the sections are formed by quasi-octagons with the elements distributed differently and with different number of elements also.

Finally, it can be seen in Figure 4 (right plot) that the cross sections evolve more uniformly when advancing from x/D = 0.01 to x/D = 0.05. The section x/D = 0.01 is not an octagon, but a polygon with much more elements forming the surface mesh. The number of elements increases rapidly.
These plots show clearly that the tip nose generated with this method is irregular and not symmetric. The roughness and microscopic irregularities, particularly in the tip region, are sources of a convective instability and may induce an important effect of the body orientation angle in the normal and lateral forces on the missile, as it has been widely demonstrated in many experiments [1], [7], [8].
Regarding the effects of irregularities, it is worth noting the work of Kumar *et al.* [7], [18], [19], [20], [21]. Experimental and numerical calculations have been done, adding perturbations of lower size than the boundary layer thickness in order to evaluate the effects of the orientation angle on the forces.

DOI: 10.13009/EUCASS2022-6087

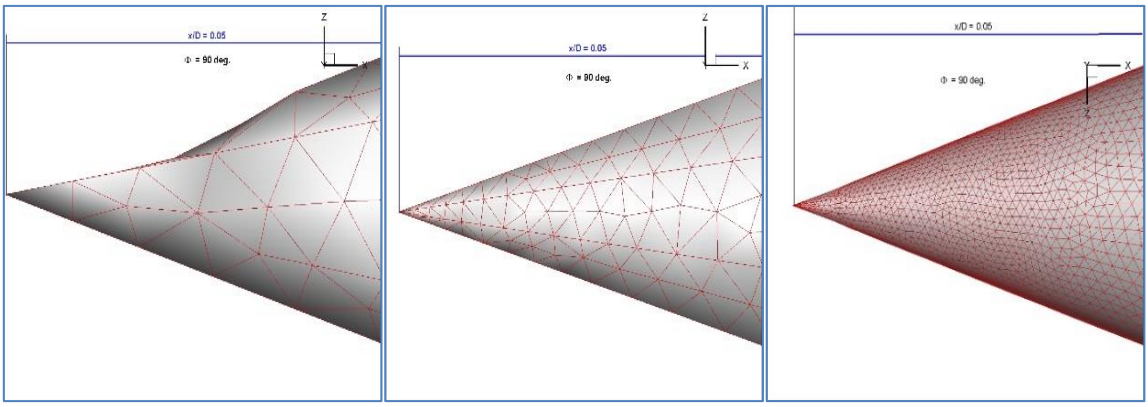

Figure 3: Detail of the unstructured grid at x/D < 0.05. Left: mesh generated with m = 3. Center: Mesh generated with m = 8. Right: finer mesh generated with m = 8.

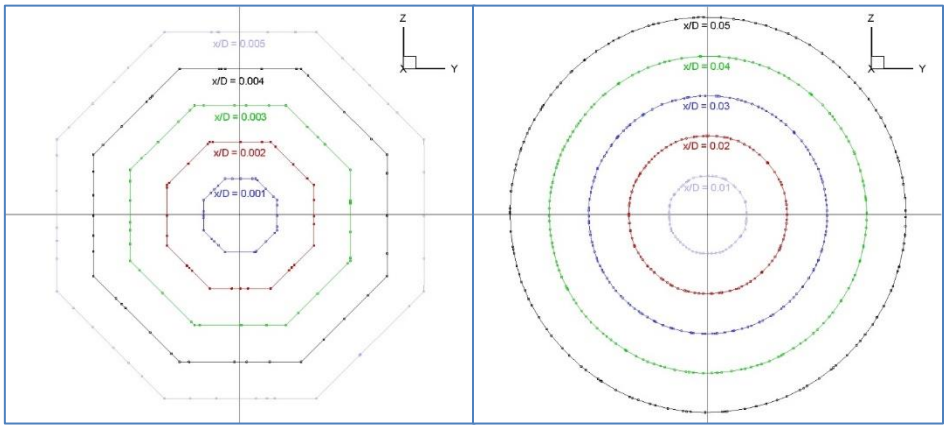

Figure 4: Left: Surface mesh cross sections at x/D = 0.001 to x/D = 0.005. Right: Surface mesh cross sections at x/D = 0.01 to x/D = 0.05. Unstructured grid.

These experimental and numerical studies show that very small imperfections of the geometry, of boundary layer thickness size can produce significant increment of the flow asymmetry and then, large lateral forces.
Prior to the calculations with the unstructured grid, an evaluation of the irregularities of the grid was done.
In order to quantify these differences a 'numerical roughness' is defined in the following manner:
First of all, as the test model is a body of revolution, the average radius at each x/D section is defined as: $r_{avg}(x) = \frac{1}{N}\sum_{i=1}^{N} r_i(x)$, being N the number of nodes at each section. Then, the 'numerical roughness' at each section is calculated with the following expression: $\overline{r_n(x)} = \frac{1}{N}\sum_{i=1}^{N} \left| r_i(x) - r_{avg}(x) \right|$ .This is an expression similar to that employed in [7]. The measurements at the different x/D sections show results of 'numerical roughness' between 40-60·10^{-6} m, i.e., $r_n/D = 40\text{-}60\cdot10^{-6}$. It should be noted that Mahadevan [7] defined a rough model with values of $Ra/D > 60\cdot10^{-6}$. On the other hand, at flight conditions of Mach number Ma = 0.2, Reynolds number Re = 2·10^6 and angle of attack 45 degrees, the crossflow boundary layer thickness close to the separation (at orientation angles close to 90 or -90 degrees) was of order $\delta/D \approx 0.006 - 0.008$ at sections x/D = 3.0, 6.9 and 9.0. This value is larger than that measured in the experiment of reference [7], tested at lower velocity and Reynolds number.

It can be concluded after the first analysis of the unstructured grid that the surface mesh generated with the procedure above mentioned, seems to resemble a model with a rough surface. As the volume mesh is also conditioned for the non-symmetric surface mesh, there will be also a non-symmetric volume mesh. The existence of a prismatic layer and tetrahedral elements in regions with strong pressure gradients and vortices of large strengths, may increase these

DOI: 10.13009/EUCASS2022-6087

irregularities effects coming from the surface. Therefore, orientation angle effects on the lateral forces can be predicted if the mesh resembles a rough model, while the structured grid can resemble a polished body, due to the axisymmetric nature of this mesh.

4. CFD validation: Turbulence modelling

The first calculations carried out for the structured grid with *ANSYS FLUENT*© code used a two-equation eddy viscosity model –the well-known *k-ω SST* model- and a Reynolds stress turbulence model (*RSM*). Both calculations at the reference condition of angle of attack 45 degrees indicated important differences in global coefficients. The value of the normal force coefficient obtained with *RSM* model was 20 % larger than that of the *k-ω SST* model. The former value was closer to the experimental value. But, both solutions were steady solutions. No transient calculations were done. Transient calculations were later done and the global coefficients achieved a stationary solution using both models.
An important conclusion is obtained after checking the side force coefficient evolution in Figure 5. The calculations were done with the ω-based *RSM* model. Assuming steady calculations (red lines in the figure), the large oscillations indicate difficulties of convergence and possibly, a time dependent solution. Using the final flow field as initial solution, transient computations were done. The solution with the lower time step $-\Delta t = 5 \cdot 10^{-4}$ s- (purple line in the figure) led to small values of the Courant-Friedrichs-Levy number (CFL) in the boundary layer region and a stationary solution with small fluctuations of the coefficient. This is a more accurate solution, with lower numerical spurious oscillations.
Moreover, the local force coefficients (side and normal force coefficients versus longitudinal coordinate) showed little damping of the values at the rear region, as it was shown by the experimental data. Additionally, the solutions with the unstructured grid, which has a large numerical roughness (defined in the previous chapter), achieved a flow region at the nose where the forces were orientation angle dependent, though ranging in a narrow envelope; while the solution at the rear was strongly dependent on the orientation angle, leading to very different flow patterns in this zone. At some orientation angles, the local side force has three or four additional peaks in its pattern after a maximum close to the central zone of the body, while at other orientation angles there were only two or three peaks. In the nose region, the flow pattern was more similar, with some differences in the position of the peaks, indicating a vortex shedding at different locations.

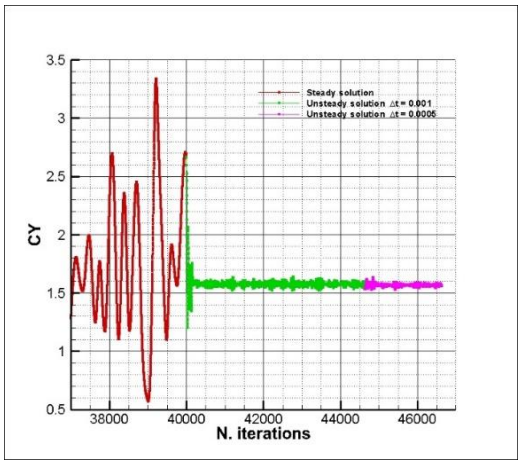

Figure 5: Side force coefficient versus number of iterations at Mach number Ma = 0.2, Reynolds number $\mathrm{Re} = 2 \cdot 10^6$ and angle of attack $\alpha = 45$ degrees: Steady and transient calculations for two time steps. Structured grid.

There was no experimental information about the orientation angle effect on the forces, just only one experimental local force at a certain orientation angle. But, the absence of damping of the forces and the conclusions of other experiments [4], [8], [9], which showed an unsteady flow region in the rear for bodies of similar fineness ratio, led us to the conclusion that neither *k-ω SST* turbulence model nor *RSM* turbulence model provided accurate enough solutions. The main features of the flow field were not completely captured.

The next step was to use *SAS* method.
SAS method is implemented in *ANSYS FLUENT*© code for ω-based turbulence models. The equation for the specific dissipation rate ω is modified introducing a second scale length, the von Karman length scale L_{vk} . Therefore, there

DOI: 10.13009/EUCASS2022-6087

were two possibilities: to use *k-ω SST-SAS* model or ω-based *RSM-SAS* model. For details, see [13], [14], [15], [16], [17]. A good description about the capabilities of the *SAS* method is given in references [13] and [17]. Calculations for a cylinder in crossflow using the *k-ω SST-SAS* instead the standard *k-ω SST* resolved the turbulent structures with better accuracy than the standard model.
In our computations, the angle of attack was 45 degrees instead of 90 degrees for a slender configuration, formed by an ogive and a cylinder of high fineness ratio.

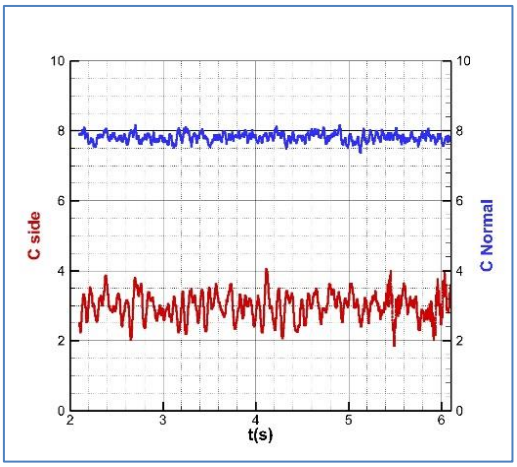

Figure 6: Time history for the side and normal force coefficients at Mach number Ma = 0.2, Reynolds number Re = $2 \cdot 10^6$ and angle of attack α = 45 degrees within a time of T = 4 s. Structured mesh. ω-based RSM-SAS model.

Thus, calculations with *k-ω SST-SAS* were done. Surprisingly, the solution obtained was different to that of the standard *k-ω SST* but it was qualitatively similar to that of the standard *RSM* model. The solution was steady and the local force coefficients did not show damping at the rear. The solution obtained with the ω-based *RSM-SAS* model was much more different. It showed time dependent solutions for the global coefficients values, with a clear periodic fluctuation. The damping of the forces were obtained at the rear. To show that, the time history of the global forces are plotted in Figure 6. While the normal force coefficient has small fluctuations, the fluctuations of the side force are important, ranging from the smaller values of 2 to values close to 4, with an averaged value of 2.99 within this period (T = 4 s). The fluctuations of the normal force are one order of magnitude lower. A Power Spectral Density (PSD) analysis of the forces shows energy content for frequencies below 20 Hz, being 7.3 Hz the dominant frequency for the side force coefficient, indicating a Strouhal number of 0.150. In reference [10], it is mentioned that the experimental Strouhal number for this test case was 0.160. The time step used was again $\Delta t = 5 \cdot 10^{-4}$ s. Several solutions at different times within a transient period of T = 0.1 s are shown in Figure 7.

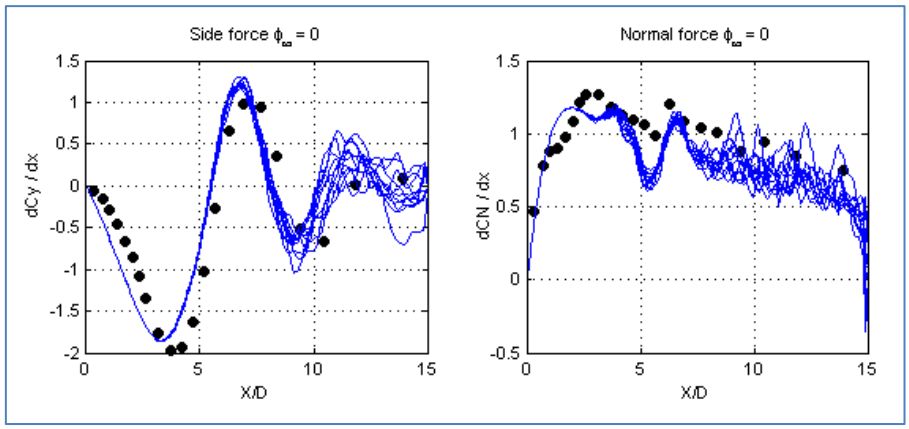

Figure 7: Several local side and normal force coefficients at Mach number Ma = 0.2, Reynolds number Re = $2 \cdot 10^6$ and angle of attack α = 45 degrees taken within a period of T = 0.1 s in intervals of Δt = 0.005 s. Structured mesh. ω-based RSM-SAS model solutions and experimental data (black dots).

DOI: 10.13009/EUCASS2022-6087

The dot black circles denote experimental data. The observation of this figure is very important: There is a steady flow region in the nose region, extending from the tip up to x/D ≈ 7.0. And a rear unsteady flow region where the forces oscillate. This flow pattern coincides with the observations of Ramberg in many experiments [9]. According to Bridges (see reference [8]) and Degani *et al.* (reference [22]), for bodies of fineness ratio below L/D = 16 there are only two flow regions, one steady flow region (denoted region 3) and another unsteady flow region where there is a periodic time-dependent shedding with vortices inclined obliquely to the longitudinal axis (named as region 2). For bodies with fineness ratio larger than 20 there may exist a third unsteady flow region (denoted region 1) where there is a von Karman vortex street type flow region with averaged values of the local side force of zero. Therefore, in region 2 the local side force is damped and in region 1 the local side force reduces to average zero values. The existence of the three regions depends both on the angle of attack and on the fineness ratio. For our ogive-cylinder configuration at the angles of attack studied only two regions (region 2 and 3) have been computed.
The averaged local side and normal forces at a period of T = 0.1 s are plotted in Figure 8, compared to the available experimental values (black dot circles). There is no information about the sampling of the experimental data.
The red line indicates the solution obtained with the standard *RSM* model. It is clear that the solution differs in the rear part compared to the experimental data. The solution obtained with *k-ω SST-SAS* seems to be less accurate than the former solution, even in the nose region. It was expected a more accurate solution when using *SAS* method. The side force is smaller in the steady flow region close to the nose; and also the normal force. The solution is very similar to the solution obtained with the standard *k-ω SST*. Then, no significant improvement of the solution has been obtained using *SAS* combined with the eddy-viscosity *k-ω SST*. The key argument for this feature is given by the authors of the method –Menter amd Egorov-, who say that *SAS* relies on an instability of the flow to generate resolved turbulence. In case such an instability is not present, the model will remain in RANS mode [15]. Other possibility is that the grid is coarse and the time steps are large (leading to CFL >> 1). In this case, *SAS* will run in RANS mode [15].
But, for the *RSM-SAS* solutions an unsteady flow region at the rear has been captured, showing the damping of the local forces (see Figure 8, green lines). The grid and time steps used are the same than those used for the *k-ω SST-SAS* model. Therefore, there is some numerical mechanism using this non isotropic model which produces sufficient instability in the flow to activate the Scale Resolving Mode, which is capable to compute turbulence scales up to the grid size limit. Then, LES-like solutions are possible in the unstable region, i.e., the region at the rear part of the body. And, in the steady flow region (nose region) the side and normal forces fit better to the correspondent experimental values, indicating a more accurate capturing of the vortices strengths, which contribute to the normal and side forces.

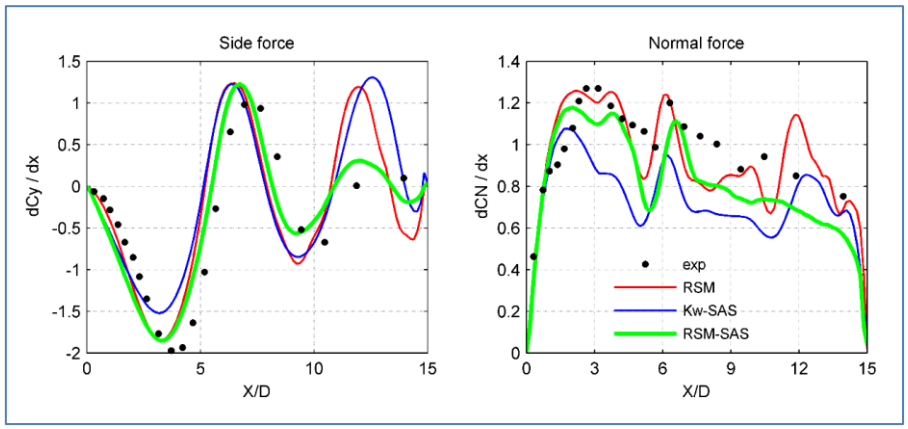

Figure 8: Averaged local side and normal force coefficients at Mach number Ma = 0.2, Reynolds number Re = $2 \cdot 10^6$ and angle of attack α = 45 degrees within a period of T = 0.1 s. Structured mesh. ω-based RSM-SAS model.

It is very illustrative to check the Figure 9, where the iso-surfaces of Q function are plotted for the two different *SAS* models used. Q function is defined as: $Q = \frac{1}{2} \cdot \left(\omega^2 - S^2 \right)$ where ω is the modulus of vorticity, an S is the strain rate.

The iso-surfaces are colored with turbulent viscosity ratio. They help to determine the coherent vortex structures. Positive Q-function values indicate areas where the rotation overcomes the strain, making possible to choose these surfaces as vortex envelopes [23]. It is very important to check that the turbulent viscosity ratio in the vortex structures is one order of magnitude lower when using the *RSM-SAS* model, regarding the solutions achieved with *k-ω SST-SAS* model.

DOI: 10.13009/EUCASS2022-6087

With the first model, RANS solutions are obtained. With the second one, LES-like solutions have been obtained. URANS methods are overly dissipative and resolve only frequencies far lower than those of turbulent fluctuations [14]. This is the reason for being less accurate in the computations of unstable or transient flows.
Therefore, the use of an advanced turbulence model, as *RSM-SAS* combined with a grid fine enough and small time steps have permitted to capture theoretically the main features of the flow for this type of configuration at a high angle of attack. The time step is very important in order to achieve CFL values close to 1. Otherwise this would lead to a steady RANS solution. A good example of this is given in [15] for a calculation using different time steps and the consequences in the accuracy of the solution.
One concern regarding the *k-ω SST-SAS* model is to check if the model runs in Scale Resolving Mode at a higher angle of attack, as the results given in [13] and [17] for a cylinder in crossflow showed good results for this model. It may be a critical angle of attack for which the flow is sufficiently unstable to activate *SAS* mode, being larger than 45 degrees. Menter *et al.* mentioned that one possibility for CFD calculations in such cases is to generate synthetic turbulence [14].
Anyway, the *RSM-SAS* model seemed to be a high level turbulence model capable to capture two separated flow regions, one steady flow region at the nose, and another unsteady flow region at the rear, in consonance with the predictions of some authors, after studying the experimental data of axisymmetric bodies of moderate to high fineness ratio [8], [9].

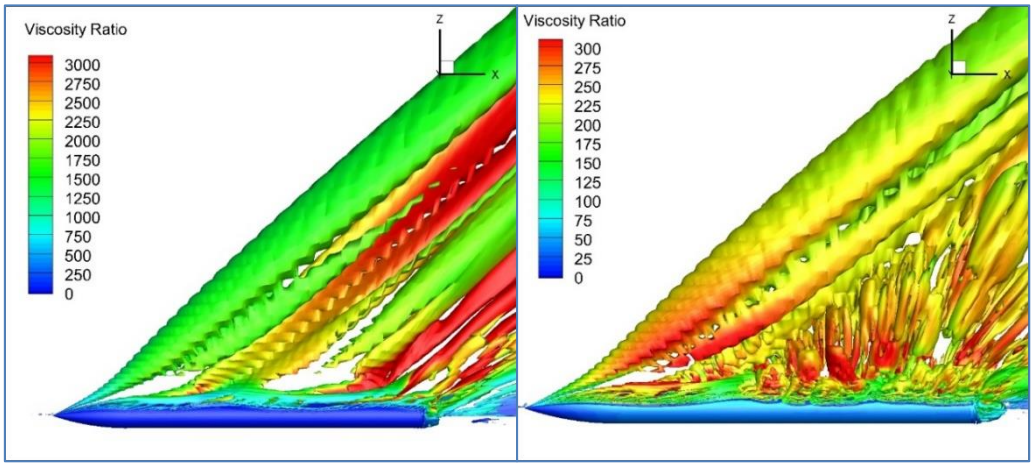

Figure 9: Iso surface of positive Q function (up to 5000) colored with turbulent viscosity ratio at Mach number Ma = 0.2, Reynolds number Re = $2 \cdot 10^6$ and angle of attack α = 45 degrees. Left: k-ω SST-SAS model. Right: ω-based RSM-SAS model. Structured grid.

A final comparison was done for pressure coefficients. There were available data for the pressure coefficients at three sections. The comparison between the theoretical solutions with the experimental values (black dots) is plotted in Figure 10 as a function of the orientation angle. For this comparison, Φ = 0 is in the leeside at the symmetry plane y = 0. There are 20 theoretical solutions, taken each $\Delta t = 5 \cdot 10^{-3}$ s within a period of T = 0.1 s.
The pressure coefficient is based in the crossflow dynamic pressure and is defined as: $Cp = \left(p - p_\infty \right) / 0.5 \cdot \left(\rho_\infty \cdot v_\infty^2 \cdot \sin^2 \alpha \right)$.

The three first regions belong to what is defined as region 3, the steady flow region close to the nose. The section x/D = 6.29 shows some oscillations of the pressure in the leeside, indicating a small fluctuation. This section lies in the transition between region 3 and region 2. There are not experimental data at the section x/D = 9.00. It can be checked that the fluctuation in the leeside, where the flow is separated and there is vortex detachment, is larger. The shape of the pressure coefficient at x/D = 9.00 tends to the shape of pressure coefficient of a cylinder in crossflow. At these conditions, there is a von Karman vortex street and the averaged local side force is zero. This is the reason for the damping of the local side force at the rear part of the body.

The conclusion of this laborious process is that there is confidence in that with fine meshes and using transient methods and an advanced turbulence model as *RSM-SAS* model, the main features of the flow past an axisymmetric body at high angle of attack can be captured with sufficient accuracy. There are two flow regions, one steady and another one unsteady, with a complex vortex sheet structure. A detailed description of this structure is given in [24].

DOI: 10.13009/EUCASS2022-6087

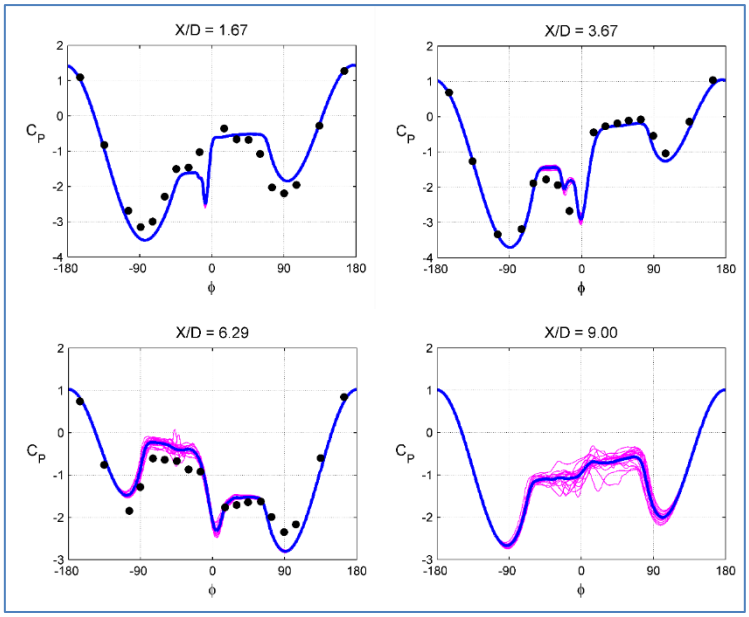

Figure 10: Pressure coefficients in circumferential direction at Mach number Ma = 0.2, Reynolds number Re = $2 \cdot 10^6$ and angle of attack α = 45 degrees within a period of T = 0.1 s at four sections. Structured mesh. ω-based RSM-SAS model solutions and experimental data (black dots).

5. Effect of angle of attack: influence of roughness

The results obtained at the conditions of Mach number Ma = 0.2, Reynolds number Re = $2 \cdot 10^6$ and angle of attack α = 45 degrees with the two grids indicate an important effect of the orientation angle on the forces if the unstructured grid is used. There is experimental evidence of the influence of the orientation angle on the forces for this ogive-cylinder configuration at other conditions of Mach number Ma = 0.5 and $Re_D = 0.3 \cdot 10^6$ [1]. The influence of the orientation angle is clearly due to a non-axisymmetric structure of the mesh and to the surface roughness in a real body. The solutions obtained with the structured grid showed no dependence on the orientation angle. The asymmetry was due to a global instability.

There is another effect of the roughness: the angle of attack for onset of asymmetry is lower for the rough model than for the smooth model. This angle was about 25 degrees for the smooth model and 15 degrees for the rough model at the conditions of Mach number Ma = 0.2 and Reynolds number Re = $2 \cdot 10^6$, according to references [1], [11]. At other Reynolds numbers, also at laminar flow conditions, this angle for onset of asymmetry is always larger for the smooth model, indicating the strong effect of the convective instability due to surface roughness or other body imperfections. Relevant information for this study is shown in reference [11]. The curves of normal and side forces are different for the smooth and rough models tested at the same facility and flow conditions. This shows clearly the effect of roughness –at a fixed orientation angle in this case- on the forces at the different incidences. The angles for onset of asymmetry are different for each model. Then, to quantify numerically this effect a sweep in angle of attack was done ranging from 10 degrees to 45 degrees.

The solution for the structured grid in terms of global force coefficients is given in Table 1, and the solution for the unstructured grid at the orientation angle of Φ = 0 deg. is shown in Table 2.

As observed in Table 1, the side force stays at small values up to an angle of attack of 34 degrees. At 34.5 degrees there is a sudden jump to larger values and beyond that the side force remains in the same range for even larger angles 40 or 45 degrees showing a ‘plateau region’ which is also seen in the experimental data. The data of Table 2 indicate asymmetric flow at 25 degrees.

The numerical data of the structured grid were compared to the experimental data of the smooth model [11]. The plots for the side force coefficient versus the angle of attack are given in Figure 11 (left side) while the results for the normal force are plotted in the right side of Figure 11. It is important to remark that for comparison with the experimental data, the negative –one of the two specular solutions- numerical solutions for the side force coefficient were used.

DOI: 10.13009/EUCASS2022-6087

Table 1: Side and normal force coefficients versus angle of attack: Ma = 0.2, Re = $2 \cdot 10^6$. Structured grid.

α (deg.)	C_Y	C_N
10	*-0.0006 ± 0.13*	*0.57 ± 0.027*
20	*-0.0005 ± 0.17*	*1.71 ± 0.019*
30	*0.13 ± 0.14*	*3.33 ± 0.065*
32.5	*-0.039 ± 0.24*	*3.83 ± 0.150*
33.5	*0.038 ± 0.24*	*4.06 ± 0.165*
34.0	*0.136 ± 0.31*	*4.36 ± 0.122*
34.5	*-2.92 ± 0.43*	*5.66 ± 0.190*
35	*2.79± 0.23*	*5.69 ± 0.076*
40	*2.81 ± 0.29*	*6.85 ± 0.09*
45	*2.99 ± 0.27*	*7.77 ± 0.10*

Table 2: Side and normal force coefficients versus angle of attack: Ma = 0.2, Re = $2 \cdot 10^6$. Unstructured grid.

α (deg.)	C_Y	C_N
20	*-0.07 ± 0.09*	*1.73 ± 0.010*
25	*-1.80 ± 0.05*	*2.69 ± 0.014*
30	*-1.96 ± 0.06*	*3.89 ± 0.050*
35	*1.32 ± 0.28*	*5.90 ± 0.090*
40	*2.19 ± 0.42*	*7.31 ± 0.120*
45	*3.22 ± 0.35*	*7.80 ± 0.120*

Champigny [1] gives a value of angle of attack for onset of asymmetry of 15-20 degrees for the smooth model but the experimental solution of Figure 11 indicates some flow instability at 20-30 degrees with the side force oscillating between negative and positive values (the two possible solutions for a bi-stable pattern). However, there is an abrupt change at 35 degrees approximately, followed by a steep slope of the curve between 35-40 degrees. At 50 degrees, a change from the negative solution to the positive solution is appreciated, likely due to the test conditions. As indicated, there are two mirror solutions, one of negative sign and the other of positive sign. A change in the free stream turbulence or oscillations of the model could be in the origin of the sudden change in sign of the side force. Beyond this angle, there is a damping of the side force. The flow is basically 'wake-like' unsteady with a small region in the nose of steady asymmetric flow.

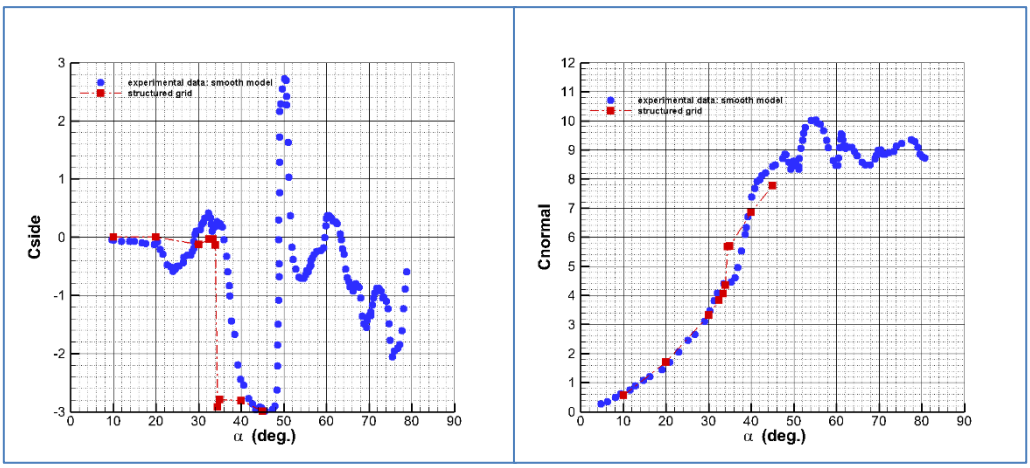

Figure 11: Left: Side force coefficient versus angle of attack. Right: Normal force coefficient versus angle of attack. Ma = 0.2, Re = $2 \cdot 10^6$. Structured grid solutions (red squares) compared to experimental data (in blue dots) for the smooth model (extracted from reference [11].

DOI: 10.13009/EUCASS2022-6087

Regarding the numerical simulations, an abrupt change from a quasi-symmetric steady flow solution at 34 degrees to an asymmetric unsteady flow solution at 35 degrees is clearly appreciated. This change from symmetric flow to asymmetric flow is also appreciated in the normal force coefficient curve of Figure 11, with an increment of the slope of the curve between 30 and 35 degrees. This is the angle of attack for onset of asymmetry when using the structured grid. The values of the side force at 35, 40 and 45 degrees are similar, following the experimental trend which anticipates a variation in the local side force pattern, changing from 3 to 4 maxima of the sinusoidal curve. This is also appreciated in the decreasing normal force slope at these angles. The semi apex angle for this ogive is $\delta_n = 18.94\,\text{deg}$. thus the empirical angle of attack for onset of asymmetry is approximately $\alpha_{onset} = 37.88\,\text{deg}$. This is close to the value obtained theoretically and in the experiments (see Figure 11).

Regarding the unstructured grid solutions, the theoretical values of side force coefficient and normal force coefficient are compared in Figure 12 left, and Figure 12 right, respectively, with their correspondent experimental data of the rough model [11]. Again, the negative numerical side force solutions were used for comparison with the experimental data. The experimental data clearly show an onset of asymmetry for an angle of attack below 20 degrees. At angle of attack of 20 degrees the side force is significant. According to Champigny [1] the value for the angle of attack of onset for asymmetry may be 12-15 degrees. According to this numerical simulation, this occurs between 20 and 25 degrees. The increment of the normal force slope at the angle of attack for onset is not as large as that of the experimental smooth body, even compared to the structured grid solution. Anyway, the onset angle is smaller than that of the smooth body indicating that the surface and flow irregularities trigger the appearance of asymmetric flow due to perturbations.

It is worth noting that the experimental side force (absolute value) is larger at 20 degrees than at 25 degrees. After this, the side force increases its absolute value, until reaching a maximum at 50 degrees.

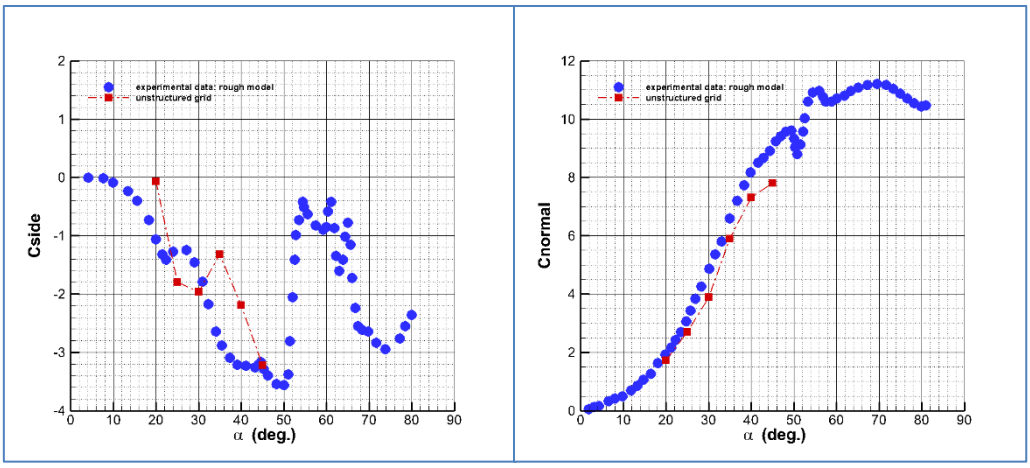

Figure 12: Left: Side force coefficient versus angle of attack. Right: Normal force coefficient versus angle of attack. Ma = 0.2, Re = $2 \cdot 10^6$. Unstructured grid solutions (red squares) compared to experimental data (in blue dots) for the rough model (extracted from reference [11]).

The reason of this behavior lies in the shape of the local side force coefficients as a function of the longitudinal coordinate. In reference [11] the curves of the experimental local side force coefficients of the rough model are plotted for the angles of attack 20 to 60 degrees. At 20 degrees, the local side force has a wavy form with two peaks before reaching the end of the body. At 30 degrees there are three maximum values. The balance is an overall side force of absolute value at 30 degrees lower than at 20, due to the change from one maximum to two maxima, alternating positive and negative local contributions to the overall side force. At 40 degrees a fourth peak appears. The base condition breaks showing a fifth peak, which is appreciated at 45 degrees. The unsteady wavy flow region advances from the rear to the nose as the angle of attack increases. At 45 degrees, this unsteady region covers the rear part of the body. The experimental data at 50 degrees indicate a similar form of the curve than at 45 degrees but as the unsteady region advances, the local side force is damped and the overall side force reaches a maximum. After 50 degrees, the global side force reduces its value compared to the maximum values at 45-50 degrees. At 55 degrees, the local side force has 6 peaks and the unsteady region is dominant, except in the nose region. There is a stall of the normal force at 50-65 degrees. At these conditions, there must be an alternating von Karman vortex street in the rear part, with average side force zero. The side force is only due to the nose contribution.

DOI: 10.13009/EUCASS2022-6087

6. Conclusions

The flow past an axisymmetric body at high angle of attack and low velocity is a challenging problem for numerical simulations. This type of flow depicts characteristics of an unsteady asymmetric flow. A dependence of the forces on the orientation angle is observed in several experiments, provided the body has geometrical irregularities.

The numerical simulation has been a complicated process assuming only URANS computations. Only the calculations with Reynolds Stress turbulence models and Scale-Adaptive Simulation method (*RSM-SAS*) captured the main features of the flow, contrary to other eddy-viscosity turbulence models or standard Reynolds Stress turbulence models. These models are so diffusive and were not capable to detect the unsteady nature of the flow at the rear and to capture small turbulent scales, unlike *RSM-SAS* model, which was capable for this up to the grid size limit. The use of LES methods for these high Reynolds flows are out of the capacities of the computational resources of our institutions. But, *RSM-SAS* has demonstrated to obtain LES-like solutions, a very important feature in order to carry out studies of missile type configurations at different regimes and at high angles of attack. The abundant experimental information of a configuration, together with the relevant conclusions of many other experiments for these type of bodies, have helped in the validation process.

It was necessary and imperative the use of fine meshes, and transient calculations with small time steps. The use of a structured axisymmetric grid together with and unstructured grid -which shows geometrical irregularities in the tip nose together with other microscopic irregularities- has become fundamental in order to check the influence of the geometrical irregularities for the existence of a convective instability which is added to a global instability at high angles of attack.

A very relevant conclusions is that using a structured grid it is possible to reproduce solutions with global coefficients close to the experimental values and that reproduce the experimental observations for a polished model. As expected from symmetry considerations, the orientation angle of the missile respect to the flow stream has no relevant effects on the results and there is an onset for the angle of attack leading to asymmetric flow. A global instability leads to a bi-stable pattern of two equivalent specular asymmetric flow solutions, one mirror of each other. The flow field on the rear part of the body is unsteady, with the amplitude of the oscillations increasing with the angle of attack. In the fore body the nose effects are dominant and there is a steady asymmetric flow. Flow instabilities lead to an asymmetric flow pattern from the tip on.

On the other hand, the surface mesh of the unstructured grid has some irregularities resembling the roughness of an irregular body. A convective (or spatial) instability exists and its effect is to reduce the angle of attack for onset of asymmetry and to produce a stronger dependence of the forces with the orientation angle. This effect is added to the global instability.

Comparison of the local and global forces obtained with the structured and unstructured grids with experimental data corresponding to polish and rough models respectively, is qualitatively good. The theoretical angles of attack for the onset of asymmetry are different than the experimental values, but the qualitative trends of the normal and side force curves are captured with fair agreement.

Acknowledgements

This investigation was funded by the Spanish Ministry of Defense under the INTA programme “Termofluidodinámica”. The authors express their gratefulness to José Manuel Olalla-Sánchez, from the Flight Physics Department of INTA, who made procedures for the grid generation process and valuable contributions for the analysis of the flow.

References

[1] P. Champigny, “High Angle of Attack Aerodynamics”, AGARD FDP-VKI Special Course on Missile Aerodynamics, June 1994, pp 5-1-5-19.

[2] P. J. Lamont, “The complex asymmetric flow over a 3.5D ogive nose and cylindrical afterbody at high angles of attack”, AIAA 82-0053. 1982. https://doi.org/10.2514/6.1982-53.

[3] E. R. Keener, G. T. Chapman, “Similarities on vortex asymmetries over slender bodies and wings” AIAA Journal Vol. 15, no. 9, pp 1370-1372, September 1977. https://doi.org/10.2514/3.60795.

[4] B. L Hunt, “Asymmetric vortex forces and wakes on slender bodies”, AIAA Paper No. 82-1336, August 1982. https://doi.org/10.2514/6.1982-1336.

DOI: 10.13009/EUCASS2022-6087

[5] R. L. Kruse, E. R. Keener, G. T. Chapman, G. Claser, "Investigation of the asymmetric aerodynamic characteristics of cylindrical bodies of revolution with variations in nose geometry and rotational orientation at angles of attack to 58 degrees and Mach numbers to 2," NASA TM 78533, 1979.

[6] P. Champigny, "Reynolds number effect on the aerodynamic characteristics of an ogive-cylinder at high angles of attack," AIAA Paper No. 84-2176, August 1984. https://doi.org/10.2514/1984-2176.

[7] S. Mahadevan, J. Rodríguez and R. Kumar, "Effect of Controlled Imperfections on the Vortex Asymmetry of a Conical Body at High Incidence", AIAA-2017-3240, Denver, Colorado, USA, 5-9 June 2017. https://doi.org/10.2514/6.2017-3240.

[8] D. H. Bridges, "The Asymmetric Vortex Wake Problem – Asking the Right Question", AIAA-2006-3553, San Francisco, California, 5-8 June 2006. https://doi.org/10.2514/6.2006-3553.

[9] S. E. Ramberg, "The Effects of Yaw and Finite Length upon the Vortex Wakes of Stationary and Vibrating Circular Cylinders", Journal of Fluid Mechanics Vol. 128, 1983, pp. 81-107. https://doi.org/10.1017/S0022112083000397.

[10] B.B. Prananta, S. Deck, P.dÉspiney, A. Jirasek, A. Kovak, M. Leplat, C. Nottin, K. Petterson, I, Wrisdale, "Numerical Simulation of Turbulent Subsonic and Transonic Flows about Missile Configurations", Final Report GARTEUR (AD) AG42 Missile Aerodynamics, NLR-TR-2007-704, 2007.

[11] J.R. Deane, "An Experimental and Theoretical Investigation into the Asymmetric Vortex Flows Characteristics of Bodies of Revolution at High Angles of Incidence in Low Speed Flow", GARTEUR TP-019, Final Report of GARTEUR AG04, July 1984.

[12] Jiménez J., Liaño G., Castillo J.L., García-Ybarra P.L., "Roll Angle Effects on the Asymmetric Flow over Axisymmetric Bodies", *8th EUCASS Congress, European Conference for Aeronautics and Space Sciences, paper 333*, July 2019, Madrid, Spain.

[13] F.R. Menter and Y. Egorov, "A Scale Adaptive Simulation Model using Two-Equation Models" AIAA 2005-1095, Reno, Nevada, 10-13 January 2005. https://doi.org/10.2514/6.2005-1095.

[14] F. R. Menter and Y. Egorov, "The Scale-Adaptive Simulation Method for Unsteady Turbulent Flow Predictions. Part 1: Theory and Model Description", Flow Turbulence Combustion (2010) 85:113-138, June 2010. https://doi.org/10.1007/s10494-010-9264-5.

[15] F. R. Menter, J. Schütze, K.A. Kurtbatskii, M. Gritskevich and A. Garbaruk, "Scale-Resolving Simulation Techniques in Industrial CFD", AIAA-2011-3474, Honolulu, Hawaii, 27-30 June 2011. https://doi.org/10.2514/6.2011-3474.

[16] F. R. Menter, M. Kuntz and R. Bender, "A Scale Adaptive Simulation Model for Turbulent Flow Predictions", AIAA 2003-0767, Reno, Nevada, 6-9 January 2003. https://doi.org/10.2514/6.2003-767

[17] ANSYS FLUENT Theory guide, Release 19.1, ANSYS, Inc. Southpointe 2600 ANSYS Drive. Canonsburg, PA 15317, April 2018, pp 92-95.

[18] R. Kumar, T. Kumar, R. Kumar, "Role of Secondary shear-layer Vortices in the Development of Flow Asymmetry on a Cone-cylinder Body at High Angles of Incidence", Experiments in Fluids (2020), 61:215. https://doi.org/10.1007/s00348-020-03045-y.

[19] J. Taligoski, E. Fernández, R. Kumar, "Experimental Investigation of Vortex Asymmetry on a Conical Forebody at High Angles of Incidence", AIAA 2014-0051, 13-17 January 2014, Maryland, USA. https://doi.org/10.2514/6.2014-0051.

[20] J. Taligoski, A. Uzun, R. Kumar, "Numerical Investigation of Vortex Asymmetry on a Conical Forebody at High Angles of Incidence", AIAA 2014-0052, 13-17 January 2014, Maryland, USA. https://doi.org/10.2514/6.2014-0052.

[21] J. Taligoski, E. Fernández, A. Uzun, R. Kumar, "Study of the Roll Orientation Effects on Vortex Asymmetry on a Conical Forebody at High Angles of Incidence", AIAA 2015-0547, 5-9 January 2015, Florida, USA. https://doi.org/10.2514/6.2015-0547.

[22] D. Degani and M. Tobak, "Numerical, Experimental and Theoretical Study of Convective Instability of Flows over Pointed Bodies at Incidence", AIAA 91-0291, Reno, Nevada, 7-10 January 1991. https://doi.org/10.2514/6.1991-291.

[23] Yves Dubief, Franck Delcayre, "On coherent-vortex identification in turbulence", Journal of Turbulence, 1, N11, 24 January 2011, https://dx.doi.org/10.1088/1468-5248/1/1/011.

[24] J. Jiménez-Varona, G. Liaño, J.L. Castillo, P.L. García-Ybarra, "Steady and Unsteady Asymmetric Flow Regions past an Axisymmetric Body", AIAA Journal Vol 59, Nº 9 (2021), pp. 3375-3386, September 2021. https://doi.org/10.2514/1.J059987.